Supercontinuum generation in both frequency and wavenumber domains in nonlinear waveguide arrays

Truong X. Tran,[1,2,*] Dũng C. Duong,[1] and Fabio Biancalana[2,3]

[1]*Department of Physics, Le Quy Don University, 236 Hoang Quoc Viet Street, 10000 Hanoi, Vietnam*

[2]*Max Planck Institute for the Science of Light, Günther-Scharowsky-Str. 1/Bau 24, 91058 Erlangen, Germany*

[3]*School of Engineering and Physical Sciences, Heriot-Watt University, Edinburgh EH14 4AS, United Kingdom*

(Received 27 November 2013; published 21 January 2014)

We study the spatiotemporal effects in waveguide arrays with Kerr and Raman nonlinearities when a short pulse is launched into the system where both dispersive and diffractive resonant radiations can be simultaneously emitted by solitons. We show that it is possible to generate and control the supercontinuum not only in the frequency domain, but also in the wavenumber domain. This work could potentially pave the way for designing unique optical devices that generate spectrally broad supercontinua with a controllable directionality by taking advantage of the combined physics of optical fibers and waveguide arrays.

DOI: 10.1103/PhysRevA.89.013826 PACS number(s): 42.65.Wi, 42.82.Et

I. INTRODUCTION

Waveguide arrays (WAs) present a unique discrete periodic photonic system to investigate many interesting fundamental phenomena such as discrete diffraction [1,2], discrete solitons [1,3,4], and photonic Bloch oscillations [1,5–8]. In applications, two-dimensional (2D) networks of nonlinear waveguides with discrete solitons may be useful for designing signal-processing circuits [9]. Binary WAs have also been intensively used to mimic relativistic phenomena typical of quantum field theory, such as *Zitterbewegung* [10], Klein paradox [11], fermion pair production [12], and the Dirac equation in the linear regime [13]. Quite recently, the optical analog of relativistic Dirac solitons with exact analytical solutions in binary WAs was found [14], which could potentially pave the way to using binary WAs as a classical simulator of quantum nonlinear effects arising from the Dirac equation, something that is thought to be impossible to achieve in conventional (i.e., linear) quantum field theory.

Dispersive resonant radiation (DisRR), which emerges due to high-order dispersion terms, has been well explored in the last decade in the temporal case for optical fibers [15–19]. When an ultrashort pulse is launched into optical fibers, a DisRR due to phase matching between the fiber and the soliton group velocity dispersion generates one or more new frequencies [18,19]. This DisRR, together with other well-known nonlinear effects such as self- and cross-phase modulation, soliton fission [20], and stimulated Raman scattering [21], are the main ingredients of supercontinuum generation [22,23], especially in highly nonlinear photonic crystal fibers [24]. Supercontinuum generation has quickly been established as one of the most important phenomena in nonlinear fiber optics and has led to a number of important technological advances in various fields, such as spectroscopy and medical imaging [25], metrology [26], and the realization of broadband sources [27], to name just a few.

In a recent study diffractive resonant radiation (DifRR)—an analog of DisRR—has been found when a spatial soliton in the continuous-wave (CW) regime is launched into WAs [28]. We have shown in Ref. [28] that when the phase-matching condition is satisfied, a spatial soliton emits DifRR with a new, well-defined direction, i.e., transverse wavenumber. It turns out that DifRR is a universal effect which can occur in WAs not only in the CW regime, but also in the spatiotemporal case, as we have shown in Ref. [29], where a long-pulse was used. In Ref. [29] wavenumber-supercontinuum generation and compensation of the soliton self-wavenumber shift by the emitted DifRR have also been revealed.

The wavelength dependence of the coupling coefficient is large because it arises from the evanescent field overlap between adjacent waveguides. This in turn makes discrete diffraction, i.e., beam spreading, wavelength dependent. This was demonstrated dramatically when a continuum generated via a microstructure fiber was injected into a single waveguide and the spectrum of the colors in the light beam was spatially dispersed at the output of the WA made of a $LiNbO_3$ crystal with defocusing nonlinearity [30,31]. Note that in Refs. [30,31] the features of polychromatic light propagation (such as spatiospectral control, diffraction management, broadband switching, and self-trapping of polychromatic light) are investigated when the input light launched into WAs is already a spectral supercontinuum source.

Motivated by the latest achievements in DifRR studies and features of polychromatic light propagation in WAs, in this paper we first present the generalized coupled-mode equations governing the spatiotemporal effects in WAs made of silica which take into account the wavelength dependence of the coupling coefficient. Then we investigate the generation of a supercontinuum in WAs both in frequency and in wavenumber, its dynamics, and also ways to control it when short input pulses are launched into the system under various conditions.

II. GENERALIZED COUPLED-MODE EQUATIONS

Our starting point is the generalized coupled-mode equations (GCMEs) of a WA consisting of identical waveguides made of silica in the frequency domain [see Eqs. (2.1.4)–

*truong.tran@mpl.mpg.de

(2.1.5) in Ref. [23]),

$$\frac{d\tilde{A}_n}{dz} = i\left[\beta(\omega) + \Delta\beta_n^{\mathrm{NL}} - \beta(\omega_0)\right]\tilde{A}_n + i\kappa(\omega)[\tilde{A}_{n+1} + \tilde{A}_{n-1}], \quad (1)$$

where $\tilde{A}_n$ is the electric field envelope in the nth waveguide in the frequency domain, z is the longitudinal coordinate, $\beta(\omega)$ is the mode-propagation constant of identical waveguides at frequency ω, $\Delta\beta_n^{\mathrm{NL}}$ is the nonlinear contribution to the mode-propagation constant in the nth waveguide, $\beta(\omega_0)$ is the mode-propagation constant at carrier frequency ω_0, and $\kappa(\omega)$ is the frequency-dependent coupling coefficient between identical adjacent waveguides (see Refs. [23,27] for more details). Note that in most cases the coupling coefficient κ is often treated as a constant, but in this specific work, where the supercontinuum is under consideration, we would like to relax this approximation.

The above frequency-domain GCMEs can be converted to the time domain by expanding both $\beta(\omega)$ and $\kappa(\omega)$ in Taylor series around the carrier frequency ω_0, replacing $(\omega - \omega_0)$ with a time derivative while taking the inverse Fourier transform, and using the comoving frame $T = t - z/v_g$, where v_g is the group velocity at ω_0. In doing so we obtain the following GCMEs in the time domain:

$$i\partial_z A_n + D(i\partial_T)A_n + \kappa(i\partial_T)[A_{n+1} + A_{n-1}] + \gamma\left(1 + \frac{i}{\omega_0}\partial_T\right)A_n(z,T)\int_{-\infty}^{\infty} R(t')|A_n(z,T-t')|^2 dt' = 0, \quad (2)$$

where the linear dispersion operator is given by $D(i\partial_T) \equiv \frac{s|\beta_2|}{2}\partial_T^2 + \sum_{m\geqslant 3}\frac{\beta_m}{m!}[i\partial_T]^m$, with $s = +1$ $(s = -1)$ for the anomalous (normal) group velocity dispersion regime, and β_m is the mth-order group velocity dispersion coefficient. Note that the group velocity $v_g = 1/\beta_1$. Meanwhile, the operator for the coupling coefficient is given by $\kappa(i\partial_T) \equiv \sum_{m\geqslant 0}\frac{\kappa_m}{m!}[i\partial_T]^m$ and κ_m is the mth-order derivative of $\kappa(\omega)$ at carrier frequency ω_0. Here we assume that the WA consists of identical waveguides, with the nonlinear parameter of each waveguide being γ. The nonlinear response function $R(t) = (1 - f_R)\delta(t) + f_R h_R(t)$, where the first term represents the instantaneous electronic contribution, with $\delta(t)$ being the Dirac δ function, $h_R(t)$ is the Raman response function of the core, and f_R represents its fractional contribution. For silica $f_R \simeq 0.18$ and the Raman effect is included through a simple model in which $h_R(t)$ has the form $h_R(t) = \frac{\tau_1^2+\tau_2^2}{\tau_1\tau_2^2}\exp(-t/\tau_2)\sin(t/\tau_1)\Theta(t)$, where $\tau_1 = 12.2$ fs and $\tau_2 = 32$ fs [27], and $\Theta(t)$ is the Heaviside step function that ensures causality. The self-steepening effect is included through the derivative ∂_T in the nonlinear terms. Now we introduce dimensionless variables $\xi = z/L_D$, $\tau = T/T_0$, and $a_n = A_n/\sqrt{P_0}$, where the dispersion length $L_D = T_0^2/|\beta_2|$, and T_0 is related to the full width at half-maximum (FWHM) pulse duration in the case of a sech-shaped pulse as follows: $T_{\mathrm{FWHM}} \simeq 1.763T_0$ [27]. The power scale is $P_0 = 1/(\gamma L_D)$. With these new variables, Eqs. (2) are equivalent to the following dimensionless GCMEs:

$$i\partial_\xi a_n + D(i\partial_\tau)a_n + L_D\kappa(i\partial_\tau)[a_{n+1} + a_{n-1}] + \left(1 + \frac{i}{\omega_0 T_0}\partial_\tau\right)a_n\int_{-\infty}^{\infty} r(\tau')|a_n(\xi,\tau-\tau')|^2 d\tau' = 0, \quad (3)$$

where the dispersion operator now assumes the form $D(i\partial_\tau) \equiv \frac{1}{2}s\partial_\tau^2 + \sum_{m\geqslant 3}\alpha_m[i\partial_\tau]^m$, with $\alpha_m \equiv \beta_m/[m!|\beta_2|T_0^{m-2}]$, whereas the operator for the coupling coefficient now has the form $\kappa(i\partial_\tau) \equiv \sum_{m\geqslant 0}\frac{\kappa_m}{m!T_0^m}[i\partial_\tau]^m$, and the dimensionless function $r(\tau)$ is obtained by rescaling time t with T_0 in the response function $R(t)$.

Equation (3) is used later to investigate supercontinuum generation in a WA. In order to simulate Eq. (3) one needs to calculate the dispersion D and the coupling coefficient κ as functions of the wavelength. In the rest of this paper, as a practical example we specify the parameters for the WA as follows: the WA is formed by identical conventional step-index fibers with the cladding made of fused silica and the core made of silica with 1.8% dopant GeO_2. The dopant at the low concentration used here is just to ensure that the refractive index of the core (which has been well approximated with the Sellmeier equation) is slightly larger than that of the cladding. The core radius is 5 μm and the center-to-center spacing between two adjacent cores is 20 μm. Recent advances in femtosecond-laser writing technologies for WAs of fused silica (see Ref. [32]) make the above-proposed WA feasible.

With this specific WA one can calculate the coupling coefficient between adjacent waveguides as a function of the wavelength using formulas in Ref. [33]. The obtained result is shown in Fig. 1(a). One can see that the longer the wavelength, the larger the coupling coefficient κ. This is understandable because for longer wavelengths the evanescent field spreads out more into the cladding, thus leading to an increase in the coupling coefficient. This feature of the coupling coefficient is essential in the dynamics of the supercontiuum generation in the WA as shown later. The solid (blue) curve in Fig. 1(b) presents the dispersion parameter D of each individual waveguide as a function of the wavelength. The dispersion is anomalous $(D > 0)$ when $\lambda > 1.307$ μm and normal $(D < 0)$ for shorter wavelengths. The dotted (red) vertical line in Fig. 1(b) indicates the position of the cutoff

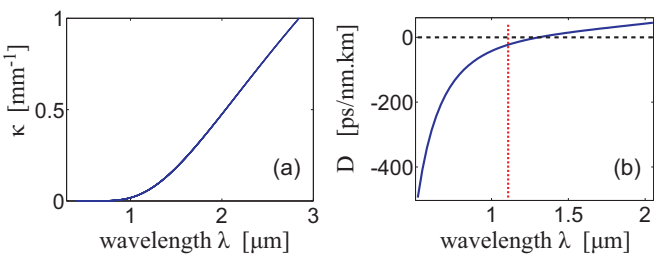

FIG. 1. (Color online) (a) Coupling coefficient κ as a function of wavelength. (b) The solid (blue) curve represents the dispersion parameter D of each individual waveguide a a function of the wavelength, whereas the dotted (red) vertical line indicates the position of the cutoff wavelength at around 1.11 μm. The parameters are given in the text.

wavelength $\lambda_{co} \simeq 1.11$ μm; thus for $\lambda > \lambda_{co}$ waveguides are single mode, whereas for shorter wavelengths they are multimode.

III. SUPERCONTINUUM GENERATION IN WAVEGUIDE ARRAYS IN BOTH FREQUENCY AND WAVENUMBER DOMAINS

In this section we systematically investigate the generation of a supercontinuum and its dynamics inside the WA when short pulses are launched into the system. The initial condition at the WA input for simulating Eqs. (3) is $a(n,\tau,0) = 3\mathrm{sech}(n/4)\exp(ik_0 n)\mathrm{sech}[(\tau+100)/2]$, where the parameter k_0 is the initial transverse wavenumber, which represents the phase difference between adjacent waveguides at the input and, thus, the initial direction of the input pulse. The input parameters are the central wavelength $\lambda_0 = 1.55$ μm and the time scale $T_0 = 50$ fs. With these input parameters, the dispersion length (also the length scale here) is calculated to be $L_D = 11$ cm and the power scale $P_0 = 9.54$ kW. The input pulse will cover seven waveguides at the FWHM level. The evolution of the pulse is illustrated in Figs. 2(a) and 2(b) in the (n,τ,ξ) space for the initial transverse wavenumber $k_0 = 1$ and 0, respectively. The top slide in Figs. 2(a) and 2(b) is shown in Figs. 2(c) and 2(d), respectively, in the (n,τ) plane on a logarithmic scale in order to enhance the visibility of weak features.

As shown in Figs. 2(a) and 2(b), after being launched into the WA, the short pulse will undergo compression both in space (n direction) and in time (τ direction). After reaching the maximum compression at the propagation distance $\xi \simeq 0.5$ the pulse will spread out quickly in both time and space. Because the input pulse with the central wavelength $\lambda_0 = 1.55$ μm is in the anomalous dispersion [see Fig. 1(b)], it will generate DisRR at wavelengths around 0.9 μm in the normal dispersion which is in perfect agreement with the phase-matching-condition calculation for the DisRR in a single fiber as shown in Ref. [18], provided that the dispersion curve plotted in Fig. 1(b) is used for this calculation. In addition to this DisRR, when the initial transverse wavenumber $k_0 = 1$ (which means the input incidence is under a certain tilt angle), as shown in Refs. [28,29], a DifRR will be generated and the anomalous recoil effect will occur. Indeed, due to the folding of the band structure at the edges of the first Brillouin zone, after the generation of the DifRR, the main pulse, instead of recoiling in the opposite direction to the DifRR, will recoil *towards* the DifRR itself [see Fig. 2(a)]. Because the direction change of the main pulse is small, the anomalous recoil effect is not very visible in Fig. 2(a) (which is a 3D plot), but it is much more visible in the case of the CW regime, for which 2D figures are illustrated in Ref. [28]. Moreover, we can confirm that the radiation generated by diffraction shown in Figs. 2(a) and 2(c), labeled " DifRR," is indeed the DifRR discovered in Ref. [28]. This can be done by going into the transverse wavenumber domain k instead of the real-space domain n as shown in Fig. 5, where the wavenumber of the obtained DifRR is in perfect agreement with the prediction by the phase-matching condition for DifRR in Ref. [28]. Now if $k_0 = 0$ (which means the incidence is normal), as shown in Ref. [28], DifRR will not occur [see Figs. 2(b) and 2(d)]. So, in the case of Figs. 2(a) and 2(c), the pulse will be split into several subpulses in both time and space (with a different direction for each subpulse in space), whereas in the case of Figs. 2(b) and 2(d) the pulse will be split just in time and spread out (but not be split into subpulses) in space [see also Figs. 3(a) and 3(b)]. Therefore,

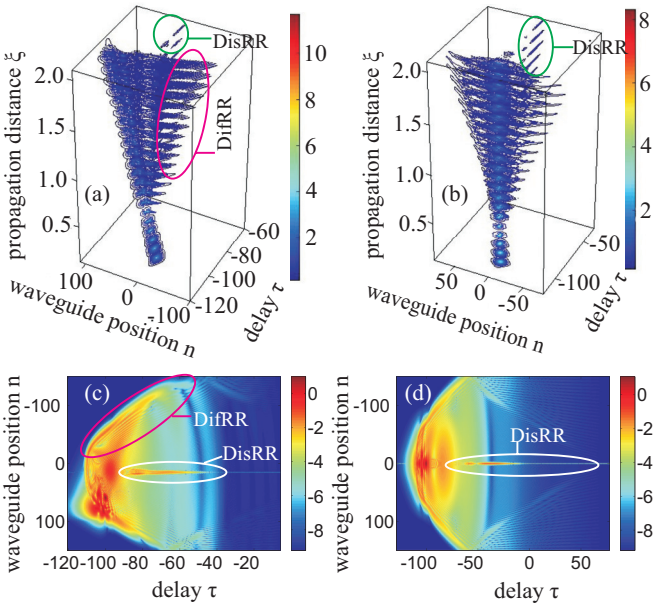

FIG. 2. (Color online) (a, b) Evolution of a pulse in the (n,τ,ξ) space when $k_0 = 1$ and 0, respectively, at a normal scale. (c, d) The top slide in (a) and (b), respectively, in the (n,τ) plane on a logarithmic scale.

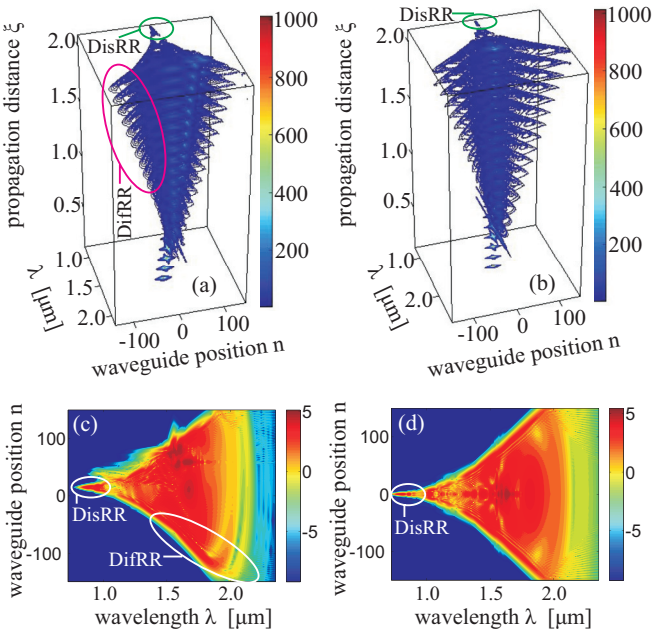

FIG. 3. (Color online) (a, b) Evolution of a pulse in the (n,λ,ξ) space when $k_0 = 1$ and 0, respectively, on a normal scale. (c, d) The top slide in (a) and (b), respectively, in the (n,λ) plane on a logarithmic scale.

by varying the tilt angle at the input, one can control the directionality of pulses formed inside the WA.

Now if we take the Fourier transform $a(n,\tau,\xi) \rightarrow \tilde{a}(n,\lambda,\xi)$ (time domain τ is transformed into wavelength domain λ), then we obtain Fig. 3 from Fig. 2. The evolution of the pulse is illustrated in Figs. 3(a) and 3(b) in the (n,λ,ξ) space for the initial transverse wavenumber $k_0 = 1$ and 0, respectively, on a normal scale. The top slide in Figs. 3(a) and 3(b) is shown in Figs. 3(c) and 3(d), respectively, in the (n,λ) plane on a logarithmic scale. One can see from Figs. 3(a) and 3(b) that at the distance $\xi \simeq 0.5$ the spectra will reach the maximum width, which corresponds to the maximum temporal compression of the pulse in Figs. 2(a) and 2(b), and at this point DisRR and the overall spectral supercontinuum will be generated in the wavelength range 0.8–2.2 μm. After reaching that distance the pulse will spread out in space. Due to the dispersion of the coupling coefficient κ shown in Fig. 1(a), the short-wavelength components have smaller coupling coefficients κ and, thus, will be dispersed less in space. On the contrary, the long-wavelength components, with larger coupling coefficients, will be dispersed strongly in space. This will lead to the formation of the Y-filled pattern in the (n,λ) plane in Figs. 3(c) and 3(d), where the bottom (top) of the letter Y corresponds to short-wavelength (long-wavelength) components. So, the short-wavelength components will be localized around the central waveguide, $n = 0$, or slightly shifted to nearby waveguides with positive (or negative) indexes ($n > 0$ or $n < 0$) depending on the initial transverse wavenumber k_0 [see Figs. 3(d) and 3(c), respectively], whereas the long-wavelength components can be strongly dispersed in space. The formation of a Y-filled pattern in the (n,λ) plane has been reported earlier, in Refs. [30,31], but in these previous works, as mentioned above, the spectral supercontinuum has been generated outside before being launched into the WA. Note that in the case $k_0 = 0$ [see Figs. 3(b) and 3(d)] the pulse will spread out in space but not be split, whereas in the case $k_0 = 1$ [see Figs. 3(a) and 3(c)] the pulse will be split into several dominant subpulses in space and these subpulses will spread out and travel farther along different directions. Note also that the DifRR will contain only long-wavelength components. This is expected because after generation the DifRR is strongly bent in space compared to the initial direction of the input pulse, and only long-wavelength components with a large coupling coefficient, as discussed earlier, can be easily bent in WAs.

Now if we take the Fourier transform $a(n,\tau,\xi) \rightarrow \tilde{a}(k,\lambda,\xi)$ (time domain τ and space domain n are transformed into wavelength domain λ and transverse wavenumber domain k, respectively), then we will obtain Fig. 4 from Fig. 2. The evolution of the pulse is illustrated in Figs. 4(a) and 4(b) in the (k,λ,ξ) space for the initial transverse wavenumber $k_0 = 1$ and $K = 0$, respectively. The top slide in Figs. 4(a) and 4(b) is shown in Figs. 4(c) and 4(d), respectively, in the (k,λ) plane. Figure 4 is plotted on a logarithmic scale. One can see from Figs. 4(a) and 4(b) that at the distance $\xi \simeq 0.5$ a supercontinuum, both in frequency and in wavenumber, will be generated, and instead of being localized in a small region at the input (k,λ) plane, the field will spread out and fill in a large region in the (k,λ) plane for $\xi > 0.5$. Note that in the case $k_0 = 0$ [see Figs. 4(b) and 4(d)], only DisRR will be generated, whereas in the case $k_0 = 1$ [see Fisg. 4(a) and 4(c)]

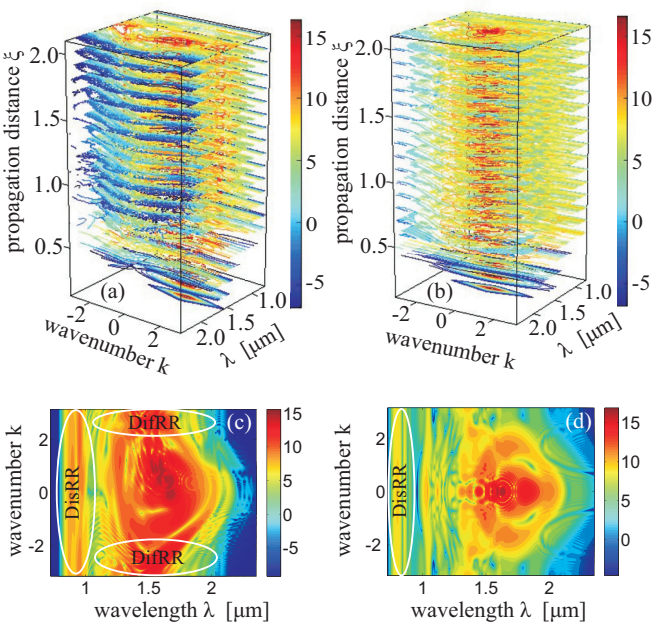

FIG. 4. (Color online) (a, b) Evolution of a pulse in the (k,λ,ξ) space when $k_0 = 1$ and 0, respectively. (c, d) The top slide in (a) and (b), respectively, in the (k,λ) plane. The figure is plotted on a logarithmic scale.

both DisRR and DifRR will be generated. It is worth noting that the central wavenumber of the DifRR for $k_0 = 1$ calculated by the phase-matching condition obtained in Ref. [28] will be $k_{\mathrm{DifRR}} \simeq -3$, i.e., close to the boundary of the Brillouin zone $k_{\mathrm{B1}} = -\pi$, and thus due to the folding effect of the Brillouin zone reported in Ref. [28] part of the DifRR will

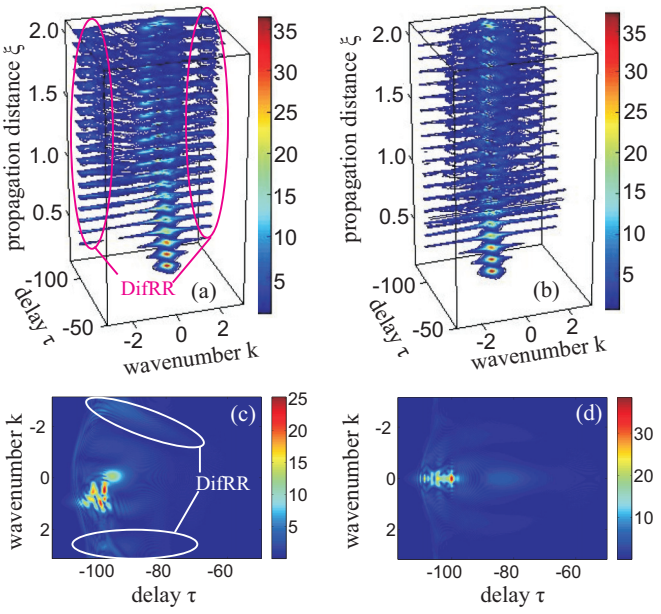

FIG. 5. (Color online) (a, b) Evolution of pulse in the (k,τ,ξ) space when $k_0 = 1$ and 0, respectively. (c, d) The top slide in (a) and (b), respectively, in the (k,τ) plane. The figure is plotted on a normal scale.

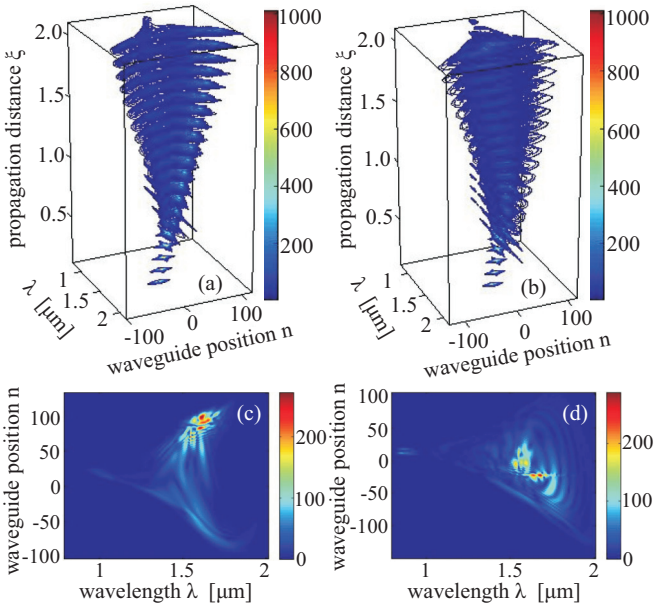

FIG. 6. (Color online) (a, b) Evolution of a pulse in the (n,λ,ξ) space when the linear potential $\alpha = 1$ and -1, respectively. (c, d) The top slide in (a) and (b), respectively, in the (n,λ) plane. The initial transverse wavenumber $k_0 = 1$. The figure is plotted on a normal scale.

be folded into the other side of the Brillouin zone ($k_{B2} = \pi$). That is why Fig. 4(c) shows two regions of DifRR at the two boundaries of the Brillouin zone. The spatial splitting of the input pulse into other subpulses and the generation of the DifRR is shown more clearly in Fig. 5(a), where the evolution of the pulse is presented in the (k,τ,ξ) space for the initial transverse wavenumber $k_0 = 1$, and in Fig. 5(c), where the top slide in Fig. 5(a) is plotted separately. The same illustration is presented in Figs. 5(b) and 5(d) for the case with initial transverse wavenumber $k_0 = 0$. Note that each value of the wavenumber k represents the direction of the corresponding pulse in space. It is clear from Figs. 5(b) and 5(d) that in the case $k_0 = 0$ the pulse is only split in time, whereas in space the pulse spreads out, but it is not split. On the contrary, in the case $k_0 = 1$ [see Figs. 5(a) and 5(c)] the splitting happens both in time and in space, and one can see that several separate dominant components of the transverse wavenumbers k are generated.

So far, we have shown that by varying the initial transverse wavenumber k_0 of the input pulse one can manipulate the propagation of pulses in space. Another way of manipulating the pulse propagation inside WAs is the application of an external linear potential across the transverse coordinate n, which changes the propagation constant in the n direction of WAs in a linear fashion, by using, for instance, the electro-optic [5] or thermal-optic [6] effect. This results in adding a term, $\alpha n a_n$, to the left-hand side of Eqs. (3), where α is the strength of the linear potential, i.e., the variation of the effective refractive index in WAs. Note that the linear potential in WAs can lead to the realization of photonic Bloch oscillations [5,6] and the compensation of the soliton self-wavenumber shift [29]. Here we show that the linear potential can be used to manipulate the supercontinuum generated inside WAs. The evolution of the pulse is illustrated in Figs. 6(a) and 6(b) in the (n,λ,ξ) space for the same initial transverse wavenumber $k_0 = 1$, but the linear potential parameter $\alpha = 1$ and -1, respectively. The top slide in Figs. 6(a) and 6(b) is shown in Figs. 6(c) and 6(d), respectively, in the (n,λ) plane. It is easy to see in Fig. 6 that one can manipulate the directions of pulses traveling inside WAs by varying α. Changing α can also lead to a slight variation of the spectral supercontinuum width; for instance, Fig. 6(d), with $\alpha = -1$, has spectral components which spread slightly farther into both short and long wavelengths compared to Fig. 6(c), with $\alpha = 1$. This also happens when the initial transverse wavenumber k_0 changes [compare the spectral widths in Figs. 3(c) and 3(d) or Figs. 4(c) and 4(d)].

IV. CONCLUSIONS

In conclusion, we have demonstrated with accurate numerical simulations that it is possible to generate a supercontinuum in WAs in both the frequency and the wavenumber domains. After a spectral supercontinuum is generated inside WAs, the short-wavelength components will be localized mainly around the input waveguides or slightly dispersed from them, whereas the long-wavelength components will be strongly dispersed in space. The input pulse can also be spatially split into several dominant subpulses inside WAs, whose directions can be controlled by varying the input angle and/or the linear potential. This work could potentially pave the way for designing unique optical devices that generate spectrally broad supercontinua with a controllable directionality and many other unexplored spatiotemporal effects in WAs.

ACKNOWLEDGMENTS

F.B. (Max Planck Research Group) and T.X.T. (Max Planck Partner Group) were supported by the German Max Planck Society for the Advancement of Science (MPG).

[1] D. N. Christodoulides, F. Lederer, and Y. Silberberg, Nature **424**, 817 (2003).
[2] A. L. Jones, J. Opt. Soc. Am. **55**, 261 (1965).
[3] D. N. Christodoulides and R. I. Joseph, Opt. Lett. **13**, 794 (1988).
[4] Y. S. Kivshar and G. P. Agrawal, *Optical Solitons: From Fibers to Photonic Crystals* (Academic Press, New York, 2003).
[5] U. Peschel, T. Pertsch, and F. Lederer, Opt. Lett. **23**, 1701 (1998).
[6] T. Pertsch, P. Dannberg, W. Elflein, A. Brauer, and F. Lederer, Phys. Rev. Lett. **83**, 4752 (1999).
[7] G. Lenz, I. Talanina, and C. M. de Sterke, Phys. Rev. Lett. **83**, 963 (1999).
[8] F. Lederer, G. I. Stegeman, D. N. Christodoulides, G. Assanto, M. Segev, and Y. Silberberg, Phys. Rep. **463**, 1 (2008).

[9] D. N. Christodoulides and E. D. Eugenieva, Phys. Rev. Lett. **87**, 233901 (2001).
[10] S. Longhi, Opt. Lett. **35**, 235 (2010).
[11] F. Dreisow, R. Keil, A. Tünnermann, S. Nolte, S. Longhi, and A. Szameit, Europhys. Lett. **97**, 10008 (2012).
[12] S. Longhi, Appl. Phys. B **104**, 453 (2011).
[13] J. M. Zeuner, N. K. Efremidis, R. Keil, F. Dreisow, D. N. Christodoulides, A. Tünnermann, S. Nolte, and A. Szameit, Phys. Rev. Lett. **109**, 023602 (2012).
[14] Tr. X. Tran, S. Longhi, and F. Biancalana, Ann. Phys. **340**, 179 (2014).
[15] H. H. Kuehl and C. Y. Zhang, Phys. Fluids B **2**, 889 (1990).
[16] P. K. A. Wai, H. H. Chen, and Y. C. Lee, Phys. Rev. A **41**, 426 (1990).
[17] V. I. Karpman, Phys. Rev. E **47**, 2073 (1993).
[18] N. Akhmediev and M. Karlsson, Phys. Rev. A **51**, 2602 (1995).
[19] F. Biancalana, D. V. Skryabin, and A. V. Yulin, Phys. Rev. E **70**, 016615 (2004).
[20] A. V. Husakou and J. Herrmann, Phys. Rev. Lett. **87**, 203901 (2001).
[21] V. N. Serkin, T. L. Belyaeva, G. H. Corro, and M. A. Granados, Quantum Electron. **33**, 325 (2003).
[22] J. M. Dudley, G. Genty, and S. Coen, Rev. Mod. Phys. **78**, 1135 (2006).
[23] G. P. Agrawal, *Applications of Nonlinear Fiber Optics*, 2nd ed. (Academic Press, New York, 2008).
[24] P. St. J. Russell, Science **299**, 358 (2003).
[25] Edited by R. Alfano, *The Supercontinuum Laser Source* (Springer-Verlag, Berlin, 2006).
[26] R. Holzwarth, M. Zimmermann, Th. Udem, T. W. Hánsch, P. Russbüldt, K. Gäbel, R. Poprawe, J. C. Knight, W. J. Wadsworth, and P. St. J. Russell, Opt. Lett. **26**, 1376 (2001).
[27] G. P. Agrawal, *Nonlinear Fiber Optics*, 5th ed. (Academic Press, New York, 2013).
[28] Tr. X. Tran and F. Biancalana, Phys. Rev. Lett. **110**, 113903 (2013).
[29] Tr. X. Tran and F. Biancalana, Opt. Express **21**, 17539 (2013).
[30] D. N. Neshev, A. A. Sukhorukov, A. Dreischuh, R. Fischer, S. Ha, J. Bolger, L. Bui, W. Krolikowski, B. J. Eggleton, A. Mitchell, M. W. Austin, and Y. S. Kivshar, Phys. Rev. Lett. **99**, 123901 (2007).
[31] A. A. Sukhorukov, D. N. Neshev, and Y. S. Kivshar, Opt. Express **15**, 13058 (2007).
[32] A. Szameit, D. Blömer, J. Burghoff, T. Pertsch, S. Nolte, and A. Tünnermann, Appl. Phys. B **82**, 507 (2006).
[33] R. Tewari and K. Thyagarajan, J. Lightwave Technol. **4**, 386 (1986).